Functional Mixed Effects Models for Imaging Genetic Data : Supplementary Document

This supplementary document include Stage II, proof of Theorem 1, wild bootstrap procedure, and detailed information of simulation setting and real data analysis for reader's reference. It includes the descriptive statistics of signal-to-noise ratio (SNR), names and corresponding MAFs of SNPs, demographic information of the selected genes PICALM, CR1, and CD2AP and names and sizes in number of voxels of detected brain regions for 3 selected genes.

Stage II

Similar to Stage I, the key idea of AET is to build a sequence of $L(\boldsymbol{\beta}(v)|\mathbf{Y}, B(v,h))$ for $h_0 = 0 < h_1 < \cdots < h_S = r_0$ at each voxel $v \in \mathcal{V}$ and then sequentially determine adaptive weights $\omega_\beta(v, v'; h_s)$ for all $v' \in B(v, h_s)$ based on $\{\hat{\boldsymbol{\beta}}(v', h_{s-1}) : v' \in B(v, h_s)\}$ for all $v \in \mathcal{V}$ and $s = 1, \ldots, S$. A path diagram of AET for $\boldsymbol{\beta}(v)$ is given as follows:

$$
\begin{array}{ccccccc}
h_0 = 0 & < & h_1 & < & \cdots & < & h_S = r_0 \\
B(v,h_0) = \{v\} & \subset & B(v,h_1) & \subset & \cdots & \subset & B(v,h_S) \\
\Downarrow & & \Downarrow & \nearrow & \cdots & \nearrow & \Downarrow \\
\{\hat{\Sigma}_Y(v) : v \in \mathcal{V}\} & & \omega_\beta(v,v';h_1) & & \cdots & & \omega_\beta(v,v';h_S = r_0) \\
\Downarrow & \nearrow & \Downarrow & \nearrow & \cdots & \nearrow & \Downarrow \\
\{\hat{\boldsymbol{\beta}}(v) : v \in \mathcal{V}\} & & \{\hat{\boldsymbol{\beta}}(v;h_1) : v \in \mathcal{V}\} & & \cdots & & \{\hat{\boldsymbol{\beta}}(v;h_S) : v \in \mathcal{V}\}.
\end{array}
$$

Since many key tuning parameters in this AET procedure are similar to those used in Stage I, we just highlight several key differences as follows.

To estimate $\boldsymbol{\beta}(v)$ at voxel v, we utilize all the data $\{\mathbf{Y}(v') : \ v' \in B(v,h)\}$ to construct the weighted log-likelihood function for a voxel v at scale h, which is given by

$$
\ell_{obs}(\boldsymbol{\beta}(v); h) = -0.5 \sum_{i=1}^{n} \sum_{v' \in B(v,h)} \omega_\beta(v, v'; h) \{\mathbf{Y}(v') - \mathbf{X}\boldsymbol{\beta}(v)\}^T \hat{\Sigma}_Y(v')^{-1} \{\mathbf{Y}(v') - \mathbf{X}\boldsymbol{\beta}(v)\}. \tag{1}
$$

By directly maximizing $\ell_{obs}(\boldsymbol{\beta}(v); h)$, we can obtain the maximum weighted likelihood estimate of $\boldsymbol{\beta}(v)$, denoted by $\hat{\boldsymbol{\beta}}(v; h)$, which is given by

$$\{\Sigma_{n,1}(v; h)\}^{-1}\mathbf{X}^T \sum_{v' \in B(v,h)} \omega_\beta(v, v'; h)\{\hat{\Sigma}_Y(v')\}^{-1}\mathbf{Y}(v'), \tag{2}$$

where $\Sigma_{n,1}(v; h) = \sum_{v' \in B(v,h)} \omega_\beta(v, v'; h)\mathbf{X}^T\{\hat{\Sigma}_Y(v')\}^{-1}\mathbf{X}$. The covariance matrix of $\hat{\boldsymbol{\beta}}(v; h)$ can be approximated by

$$\mathrm{Cov}(\hat{\boldsymbol{\beta}}(v; h)) \approx \Sigma_n(\hat{\boldsymbol{\beta}}(v; h)) = \{\Sigma_{n,1}(v; h)\}^{-1}\mathbf{X}^T\Sigma_{n,2}(v; h)\mathbf{X}\{\Sigma_{n,1}(v; h)\}^{-1}, \tag{3}$$

where $\Sigma_{n,2}(v; h)$ is given by

$$\sum_{v', v'' \in B(v,h)} \omega_\beta(v, v'; h)\omega_\beta(v, v''; h)\hat{\Sigma}_Y(v')^{-1}\{\mathbf{Y}(v') - \mathbf{X}\hat{\boldsymbol{\beta}}(v')\}\{\mathbf{Y}(v'') - \mathbf{X}\hat{\boldsymbol{\beta}}(v'')\}^T\hat{\Sigma}_Y(v'')^{-1}.$$

The adaptive weights are given by

$$\omega_\beta(v, v'; h) = K_{loc}(||v - v'||_2/h)K_{st}(D_\beta(v, v'; h)/C_n), \tag{4}$$

where $D_\beta(v, v'; h_{s-1})$ is set as

$$\{\hat{\boldsymbol{\beta}}(v; h_{s-1}) - \hat{\boldsymbol{\beta}}(v'; h_{s-1})\}^T\{\mathrm{Cov}(\hat{\boldsymbol{\beta}}(v))\}^{-1}\{\hat{\boldsymbol{\beta}}(v; h_{s-1}) - \hat{\boldsymbol{\beta}}(v'; h_{s-1})\}. \tag{5}$$

Based on $\hat{\boldsymbol{\beta}}(v; h)$, we can further construct test statistics to examine scientific questions regarding $\boldsymbol{\beta}(v)$. These questions can be formulated as linear hypotheses about $\boldsymbol{\beta}(v)$,

$$H_{0,\mu} : R_1\boldsymbol{\beta}(v) = \mathbf{b}_0 \quad \text{vs.} \quad H_{1,\mu} : R_1\boldsymbol{\beta}(v) \neq \mathbf{b}_0, \tag{6}$$

where $\mu = R_1\boldsymbol{\beta}(v)$, R_1 is a $r \times k$ matrix of full row rank and b_0 is a $r \times 1$ specified vector. We test the null hypothesis $H_{0,\mu} : R_1\boldsymbol{\beta}(v) = b_0$ using the Wald test statistic

$$W_\mu(v; h) = \{R_1\hat{\boldsymbol{\beta}}(v; h) - \mathbf{b}_0\}^T\{R_1\Sigma_n(\hat{\boldsymbol{\beta}}(v; h))R_1^T\}^{-1}\{R_1\hat{\boldsymbol{\beta}}(v; h) - \mathbf{b}_0\}. \tag{7}$$

Under $H_{0,\mu}$, $W_\mu(v; h)$ is asymptotically distributed as $\chi^2(r)$ (**?**).

Proof of Theorem 1

It is shown that the REML estimation of covariance is invariant to the choice of K_x (Searle et al, 1992, Ch.6). Without loss of generality, we may assume $K_x K_x^T = \boldsymbol{I}_{n-p}$, where $\boldsymbol{I}_{n-p}$ is an $(n-p) \times (n-p)$ identity matrix. Also, since the matrix $K_x \boldsymbol{Z}^T \boldsymbol{I}_L \boldsymbol{Z} K_x^T = \Omega$ is positive semidefinite, there exists an $(n-p) \times (n-p)$ orthogonal matrix U and a diagonal matrix $D_0 = \text{diag}\{d_1, \ldots, d_{n-p}\}$ such that $\Omega = U D_0 U^T$, where the columns of U are the eigenvectors of Ω and $d_i, i = 1, \cdots, n-p$ are the corresponding eigenvalues. Under the null hypothesis $\sigma_\gamma^2(v) = 0$, $\boldsymbol{Y}^*(v')$ is distributed as $N(0, \sigma_e^2(v')\boldsymbol{I}_{n-p})$. Therefore, we have the following results:

- $\sigma_e(v')^{-1} U^T \boldsymbol{Y^*}(v') \overset{d}{\sim} N(\boldsymbol{0}_{n-p}, \boldsymbol{I}_{n-p})$ and $\frac{1}{\sigma_e(v')\sqrt{1+\lambda(v')d_i}} u_i^T \boldsymbol{Y}^*(v') \overset{d}{\sim} N(0, \frac{1}{1+\lambda(v')d_i})$, where u_i is the ith eigenvector of Ω. Also,

$$\frac{1}{\sigma_e(v')}\{\boldsymbol{I}_{n-p} + \lambda(v')D_0\}^{-\frac{1}{2}} U^T \boldsymbol{Y}^*(v') \overset{d}{\sim} N(\boldsymbol{0}_{n-p}, [\boldsymbol{I}_{n-p} + \lambda(v')D_0]^{-1}). \tag{8}$$

- The determinant of $\sigma_e^2(v')\{\boldsymbol{I}_{n-p} + \lambda(v')\Omega\}$ equals $\sigma_e(v')^{2(n-p)} \prod_{i=1}^{n-p}\{1 + \lambda(v')d_i\}$.

- Since the actual dimension of Ω is at most L, we have $d_i = 0$ for $i = L+1, \ldots, n-p$.

Then, $\ell_{REML}(\boldsymbol{Y}^*(v') \mid \boldsymbol{Z}, \sigma_e^2(v'), \sigma_\gamma^2(v) \geq 0) - \ell_{REML}(\boldsymbol{Y}^*(v') \mid \boldsymbol{Z}, \sigma_e^2(v'), \sigma_\gamma^2(v) = 0)$ can be approximated by

$$\begin{aligned}
&\frac{1}{2\sigma_e^2(v')}(\boldsymbol{Y}^*(v')^T \boldsymbol{Y}^*(v') - \boldsymbol{Y}^*(v')^T\{U[\boldsymbol{I}_{n-p} + \lambda(v')\Omega]U^T\}^{-1}\boldsymbol{Y}^*(v')) - \frac{1}{2}\sum_{i=1}^{L}\log(1+\lambda(v')d_i) \\
&\overset{\mathcal{D}}{=} \frac{1}{2}\{\sum_{i=1}^{n-p} z_i^2(v') - \sum_{i=1}^{L}\log(1+\lambda(v')d_i) - \sum_{i=1}^{n-p}\frac{z_i^2(v')}{1+\lambda(v')d_i}\} \\
&\overset{\mathcal{D}}{=} \frac{1}{2}\{\sum_{i=1}^{L}\frac{z_i^2(v')\lambda(v')d_i}{1+\lambda(v')d_i} - \sum_{i=1}^{L}\log(1+\lambda(v')d_i)\} = \frac{1}{2}\, D(v'),
\end{aligned} \tag{9}$$

where the $z_i(v')$'s are mutually independent for all $i = 1, \cdots n-p$ and normally distributed with mean 0 and variance 1. Finally, we have

$$\begin{aligned}
\mathrm{RLRT}_n(v) =& \ 2 \sup_{\sigma^2_\gamma(v)\geq 0} \{L_{REML}(\sigma^2_\gamma(v) \mid \boldsymbol{Y^*}, B(v,h)) - L_{REML}(0 \mid \boldsymbol{Y^*}, B(v,h))\} \\
=& \ 2 \sup_{\sigma^2_\gamma(v)\geq 0} \sum_{v'\in B(v,h)} \omega(v,v',h)\{\ell_{REML}(\boldsymbol{Y}^*(v') \mid \boldsymbol{Z}, \hat{\sigma}^2_e(v'), \sigma^2_\gamma(v) > 0) \\
& - \ell_{REML}(\boldsymbol{Y}^*(v') \mid \boldsymbol{Z}, \hat{\sigma}^2_e(v'), \sigma^2_\gamma(v) = 0)\} \\
\overset{\mathcal{D}}{=}& \sup_{\sigma^2_\gamma(v)\geq 0} \{ \sum_{v'\in B(v,h)} \omega(v,v',h) D(v')\}.
\end{aligned} \tag{10}$$

Wild Bootstrap Procedure

Let $\Sigma_{Y^*}(v) = \sigma^2_\gamma(v)\Omega + \sigma^2_e(v)\mathbf{I}_{n-p}$ and transform $\mathbf{Y}^*(v)$ into $\widetilde{\mathbf{Y}}^*(v) = U^T\Sigma_{Y^*}(v)^{-1/2}\mathbf{Y}^*(v)$ such that $\widetilde{\mathbf{Y}}^*(v) \sim N(\mathbf{0}, \mathbf{I}_{n-p})$. It follows from $\Omega = UD_0U^T$ that

$$\widetilde{\mathbf{Y}}^*(v) = (\tilde{y}_1(v), \cdots, \tilde{y}_{n-p}(v))^T = \{\sigma^2_e(v)\mathbf{I}_{n-p} + \sigma^2_\gamma(v)D\}^{-1/2}U^T\mathbf{Y}^*(v). \tag{11}$$

We develop a wild bootstrap procedure as follows.

- Step 1. Define a grid $0 = \lambda_1(v) < \lambda_2(v) < \cdots < \lambda_M(v)$ of M possible values for $\lambda(v)$.
- Step 2. Generate $\xi^{(s)}_l$ independently from $N(0,1)$ for $l = 1, \ldots, n-p$.
- Step 3. For every grid point $\lambda_m(v)$, calculate an approximation of $D(v'; \lambda_m(v)/\hat{\sigma}^2_e(v))$ as follows:

$$\begin{aligned}
\widehat{D}^{(s)}(v'; \lambda_m(v)/\hat{\sigma}^2_e(v)) =& \sum_{l=1}^{n-p} \frac{\xi^{(s)}_l\{\tilde{y}^2_l(v') - 1\}d_l\lambda_m(v)/\hat{\sigma}^2_e(v') + d_l\lambda_m(v)/\hat{\sigma}^2_e(v')}{1 + d_l\lambda_m(v)/\hat{\sigma}^2_e(v')} \\
& - \sum_{l=1}^{n-p} \log(1 + d_l\lambda_m(v)/\hat{\sigma}^2_e(v')).
\end{aligned} \tag{12}$$

Since the samples are generated independently among voxels which does not take the spatial correlation of the imaging measurements into consideration, the samples in

(12) are generated from the original imaging data instead in order to address this limitation.

- Step 4. Calculate

$$\mathrm{RLRT}_n^{(s)}(v) = \sup_{1\le m\le M}\{\sum_{v'\in B(v,h)} \omega(v,v';h)\widehat{D}^{(s)}(v';\lambda_m(v)/\hat{\sigma}_e^2(v'))\}. \tag{13}$$

- Step 5. Repeat Steps 1-5 for S iterations.

- Step 6. Approximate the p-value of $\mathrm{RLRT}_n(v)$ based on an approximation given by

$$\mathrm{RLRT}_n(v) \overset{D}{\approx} a_0 u_0 d_0, \tag{14}$$

where $u_0 \sim Bernoulli(1-p_0)$, $d_0 \sim \chi_1^2$ are independent random variables, $p_0 = P(u_0 = 0)$ and a_0 are unknown constants, and $\overset{D}{\approx}$ denotes approximate equality in distribution. Considering computational efficiency, instead of generating many bootstrap samples, we estimate the parameters a_0 and p_0 in the approximation (14) as follows:

$$\hat{a}_0 = \sum_{v'\in B(v,h^S)} \omega(v,v';h^S)\tilde{a}_0 \ , \quad \hat{p}_0 = \sum_{v'\in B(v,h^S)} \omega(v,v';h^S)\tilde{p}_0, \tag{15}$$

where

$$\tilde{p}_0 = 1 - 3\frac{\{\sum_{s=1}^S \mathrm{RLRT}_n^{(s)}(v)\}^2}{S\sum_{s=1}^S \mathrm{RLRT}_n^{(s)}(v)^2} \quad \text{and} \quad \tilde{a}_0 = \frac{\sum_{s=1}^S RLRT_n^{(s)}(v)}{S(1-\hat{p})}. \tag{16}$$

Computationally, the above algorithm is quite efficient. First, we only need to compute $\tilde{\mathbf{Y}}^*(v)$ once for all voxels. Second, Ω is fixed and thus it is straightforward to compute its eigenvalues and eigenfunctions. Third, all $\hat{\sigma}_e^2(v)$ are calculated once at Step I.1. Fourth, to choose grid points of $\lambda(v)$, we set $M = 50$ and $\lambda_M(v) = 3\max_{v'\in\mathcal{V}} \hat{\sigma}_\gamma^2(v')$.

Simulation Results

Table 1: Simulation setting: descriptive statistics of **SNRs** for 10 regions of $\sigma^2_\gamma(v)$ from a simulated data set of *Scenario I*, in which the SNPs are extracted from the chromosome 1 in ADNI.

$\sigma^2_\gamma(v)$	Number of voxels	Mean	Standard Deviation	Min	Max
0	4749	0.124	0.062	0.024	0.412
0.0050	207	0.819	0.572	0.003	2.745
0.0075	135	1.010	0.774	0.006	3.340
0.0100	111	1.123	0.815	0.021	3.714
0.0125	147	1.270	1.014	0.043	4.303
0.0150	75	1.262	1.026	0.025	4.074
0.0175	48	1.334	1.150	0.034	5.930
0.0200	144	1.436	1.060	0.019	3.940
0.0225	111	1.687	1.191	0.036	4.886
0.0250	81	1.877	1.366	0.020	6.674

Table 2: Simulation setting: descriptive statistics of **SNRs** for 10 regions of $\sigma^2_\gamma(v)$ from a simulated data set of *Scenario II*, in which the SNPs are extracted from the gene PICALM in ADNI.

$\sigma^2_\gamma(v)$	Number of voxels	Mean	Standard Deviation	Min	Max
0	4749	0.111	0.055	0.022	0.357
0.005	207	0.189	0.136	0.001	0.699
0.010	135	0.234	0.188	0.001	0.854
0.015	111	0.301	0.246	0.003	1.092
0.020	147	0.349	0.274	0.003	1.307
0.025	75	0.337	0.282	0.004	1.111
0.030	48	0.365	0.257	0.0005	0.996
0.035	144	0.424	0.283	0.003	1.324
0.040	111	0.491	0.443	0.010	1.008
0.045	81	0.500	0.403	0.034	1.909

Table 3: ADNI data analysis: the minor allele frequency (MAF) in % of selected SNPs on PICALM, CR1, and CD2AP

PICALM							
rs618679	22.1	rs2077815	22.6	rs666692	48.9	rs527162	22.1
rs10898427	21.2	rs11234495	24.8	rs664629	37.0	rs680119	40.7
rs510566	22.9	rs10501602	8.8	rs1774523	19.4	rs10501608	17.2
rs10501604	17.4	rs713346	25.2	rs1941375	27.3	rs10792821	21.0
rs475639	48.0	rs669336	18.8	rs677909	31.6	rs642949	37.5
rs7938033	42.7	rs10792820	25.3	rs11234532	10.2		
CR1				**CD2AP**			
rs1571344	13.7	rs2025935	31.5	rs9296559	26.9	rs9473121	32.8
rs4310446	18.1	rs11117959	19.3	rs12523687	10.0	rs9395267	10.4
rs10127904	29.4	rs650877	19.9	rs1385741	39.0	rs9296562	40.1
rs3737002	27.5	rs11118131	19.0	rs6458573	32.9	rs13191654	22.4
rs677066	21.9	rs6691117	21.8	rs3818866	26.3	rs9395285	26.6
rs3818361	19.7	rs6701713	19.7	rs6936622	11.0	rs1485780	26.9
rs12734030	17.9	rs12034383	41.0	rs1485781	32.9	rs9349417	26.9
rs1408077	19.1	rs10779339	49.7	rs10948367	26.9		

Table 4: ADNI data analysis: demographic information of the 328 subjects in the dataset investigating the effects of **PICALM**. For the *categorical* variables: gender, handedness and risk of APOE, the numbers are the frequencies for the corresponding groups. For the *continuous* variables: baseline age, baseline ICV and years of education, and the numbers are the mean (standard deviation) of each variable in each group.

		Healthy Control	Alzheimer's Disease
Total		176	152
Male (Female)		99 (77)	84(68)
Right (Left) Hand Users		163 (13)	142(10)
Risk of APOE	3	2	31
	2	41	68
	1	111	49
	0	22	4
Baseline Age		76.1 (5.1)	75.5 (7.6)
Baseline ICV		1.28×10^6 (1.24×10^5)	1.27×10^6 (1.45×10^5)
Years of Education		16.3 (2.7)	14.9 (3.2)

Table 5: ADNI data analysis: demographic information of the 299 subjects in the dataset investigating the effects of **CD2AP**. For the *categorical* variables: gender, handedness and risk of APOE, the numbers are the frequencies for the corresponding groups. For the *continuous* variables: baseline age, baseline ICV and years of education, and the numbers are the mean (standard deviation) of each variable in each group.

		Healthy Control	Alzheimer's Disease
Total		155	144
Male (Female)		84 (71)	77(67)
Right (Left) Hand Users		143 (12)	135(9)
Risk of APOE	3	3	38
	2	37	64
	1	97	49
	0	18	3
Baseline Age		76.1 (5.2)	75.1 (7.5)
Baseline ICV		1.27×10^6 (1.25×10^5)	1.27×10^6 (1.46×10^5)
Years of Education		16.1 (2.8)	14.7 (3.1)

Table 6: ADNI data analysis: the detailed significant brain regions affected by **CD2AP** using FMEM. The regions with the $*$ means the regions are detected by FMEM and voxel-based method; the regions with the $**$ means only detected by voxel-based method; the regions with # means only detected by FMEM with healthy control only; the regions with ## means detected by FMEM with AD only; $\bullet$ means not applicable.

Brain Region	Number of Voxels (right)	Number of Voxels (left)
Superior temporal gyrus	167	$\bullet$
Inferior temporal gyrus	*369	378
Precentral gyrus	*170	439
Middle frontal gyrus	127	*295
Postcentral gyrus	$60^{\#}$	183
Insula	53	74
Putamen	$*200^{\#}$	$123^{\#}$
Fusiform	$117^{\#\#}$	306
Inferior parietal but supramarginal and angular gyri	87	$\bullet$
Angular	433	$\bullet$
Inferior frontal gyrus - triangular part	*180	*79
Inferior occipital gyrus	269	$\bullet$
Superior frontal gyrus	71	$\bullet$
Supplementary Motor Area	$117^{\#}$	$\bullet$
Postcentral gyrus	*104	*183
Superior frontal gyrus and medial	188	159
Anterior cingulate and paracingulate gyri	428	88
Median cingulate and paracingulate gyri	149	$*116^{\#\#}$
Calcarine fissure and surrounding cortex	53	266
Cuneus	$151^{\#}$	345
Superior occipital gyrus	$\bullet$	317
Middle occipital gyrus	$\bullet$	*144
Precuneus	61	$\bullet$
Paracentral Lobule	86	$\bullet$
Pallidum	$\bullet$	58
Caudate	$\bullet$	197
Lingual	$\bullet$	$*114^{\#\#}$
Inferior frontal gyrus - opercular part	$\bullet$	*78
Inferior occipital gyrus	$\bullet$	133
Middle temporal gyrus	$\bullet$	394
Inferior frontal gyrus - orbital part	$\bullet$	61
Temporal pole: superior temporal gyrus	**74	$\bullet$
Temporal pole: middle temporal gyrus	**61	$\bullet$
ParaHipopcampal gyrus	$\bullet$	
Inferior parietal but supramarginal and angular gyri	$\bullet$	$\bullet$

Table 7: ADNI data analysis: the detailed significant brain regions affected by **CR1** using FMEM. The regions with the $*$ means the regions are detected by FMEM and voxel-based method; the regions with the $**$ means only detected by voxel-based method; the regions with # means only detected by FMEM with healthy control only; the regions with ## means detected by FMEM with AD only; $\bullet$ means not applicable.

Brain Region	Number of Voxels (right)	Number of Voxels (left)
Superior temporal gyrus	167	$\bullet$
Inferior temporal gyrus	$150^{\#}$	$378^{\#,\#\#}$
Precentral gyrus	$170^{\#\#}$	$*439^{\#\#}$
Middle frontal gyrus	$127^{\#,\#\#}$	$295^{\#,\#\#}$
Postcentral gyrus	60	$**65$
Insula	53	$74^{\#}$
Putamen	200	$*123$
Fusiform	$117^{\#}$	$306^{\#}$
Inferior temporal gyrus	219	$\bullet$
Inferior parietal but supramarginal and angular gyri	87	$\bullet$
Angular	433	$\bullet$
Inferior frontal gyrus, triangular part	$180^{\#}$	$*79$
Inferior occipital gyrus	269	133
Superior frontal gyrus	$71^{\#}$	$\bullet$
Supplementary Motor Area	117	$\bullet$
Postcentral gyrus	$104^{\#}$	183
Superior frontal gyrus, medial	$188^{\#}$	159
Anterior cingulate and paracingulate gyri	428	88
Median cingulate and paracingulate gyri	209	116
Calcarine fissure and surrounding cortex	$53^{\#}$	$266^{\#\#}$
Cuneus	151	$345^{\#\#}$
Superior occipital gyrus	$\bullet$	$317^{\#\#}$
Middle occipital gyrus	144	$\bullet$
Precuneus	61	$\bullet$
Paracentral Lobule	$86^{\#\#}$	$\bullet$
Pallidum	58	$\bullet$
Caudate	$\bullet$	197
Lingual	$\bullet$	$114^{\#\#}$
Inferior frontal gyrus, opercular part	$\bullet$	78
Middle temporal gyrus	$\bullet$	$*394^{\#,\#\#}$
Inferior frontal gyrus, orbital part	$\bullet$	61
Hippocampus	$\bullet$	$\bullet$
Olfactory cortex	$\bullet$	$\bullet$
Gyrus rectus	$\bullet$	$\bullet$
Rolandic Operculum	$76^{\#}$	$\bullet$
Temporal pole: superior temporal gyrus	$\bullet$	$\bullet$

Table 8: ADNI data analysis: the detailed significant brain regions affected by **PICALM** using FMEM. The regions with the $*$ means the regions are detected by FMEM and voxel-based method; the regions with the $**$ means only detected by voxel-based method; the regions with # means only detected by FMEM with healthy control only; the regions with ## means detected by FMEM with AD only; • means not applicable.

Brain Region	Number of Voxels (right)	Number of Voxels (left)
Inferior frontal gyrus - triangular part	206	•
Inferior frontal gyrus - orbital part	213	•
Insula	363	•
Hippocampus	72	•
ParaHippocampal gyrus	72	**60
Amygdala	68	•
Fusiform	205	•
Putamen	144	•
Superior temporal gyrus	790	•
Temporal pole: superior temporal gyrus	472	•
Middle temporal gyrus	441	•
Temporal pole: middle temporal gyrus	127	•
Inferior temporal gyrus	402	•
Precentral gyrus	519	•
Middle frontal gyrus	588	•
Postcentral gyrus	404#	•
SupraMarginal gyrus	350	•
Superior occipital gyrus	72	•
Middle occipital gyrus	834	•
Inferior parietal but supramarginal and angular gyri	239#	•
Angular	491	•
Rolandic Operculum	76	•
Inferior frontal gyrus - opercular part	112	•
Superior frontal gyrus - orbital part	75	•
Middle frontal gyrus	375	•
Middle frontal gyrus - orbital part	338	•
Superior frontal gyrus	66	•
Median cingulate and paracingulate gyri	•	**51

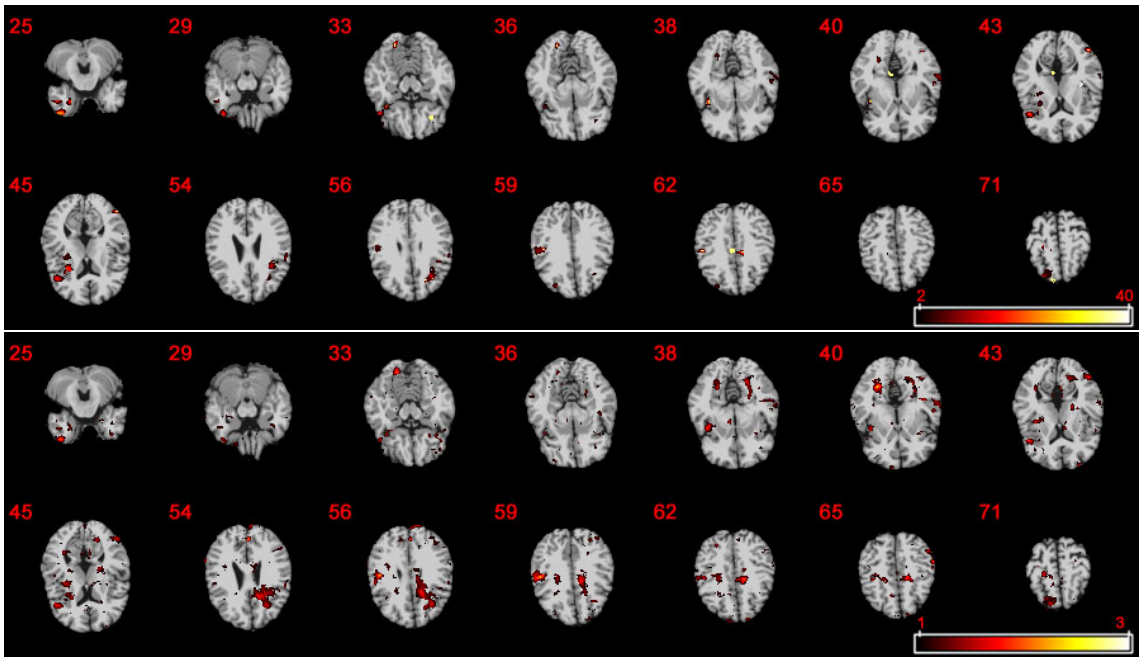

Figure 1: ADNI data analysis based on the combined HC and AD samples: the $-\log_{10}(p)$ maps for testing the genetic effect of **CD2AP** on RAVEN images by using FMEM from 14 selected slices. The first and second rows are obtained from FMEM, while the third and fourth rows are obtained from Ge's method. The colorbar of $-\log_{10}(p)$ ranges from 2 to 40 for FMEM and from 1 to 3 for Ge's method, respectively.

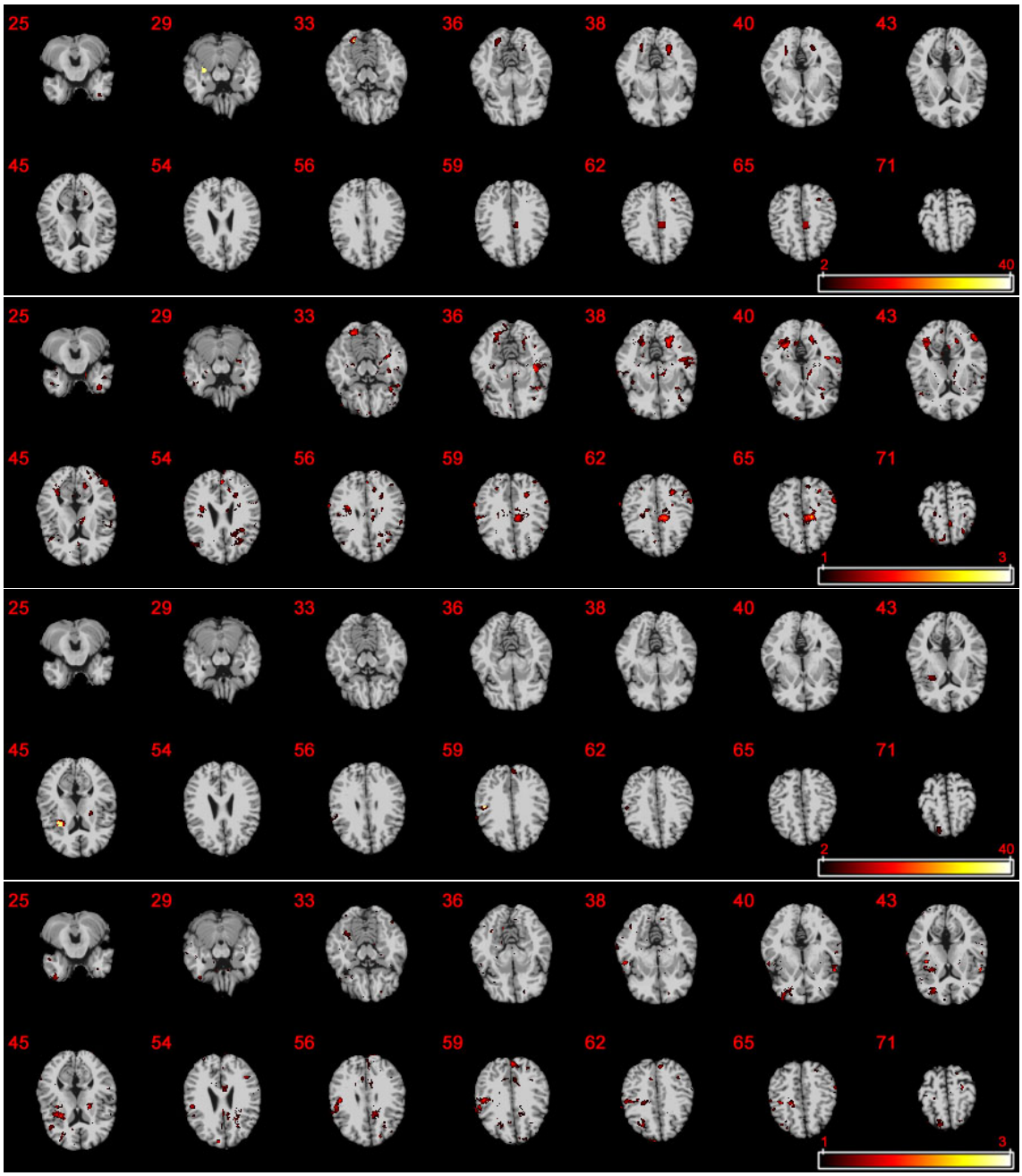

Figure 2: ADNI data analysis based on either AD samples (the first four rows) or HC samples (the last four rows): the $-\log_{10}(p)$ maps for testing the genetic effect of **CD2AP** on RAVEN images by using FMEM from 14 selected slices. The first, second, fifth, and sixth rows are obtained from FMEM, while the third, fourth, seventh, and eighth rows are obtained from Ge's method. The colorbar of $-\log_{10}(p)$ ranges from 2 to 40 for FMEM and from 1 to 3 for Ge's method, respectively.

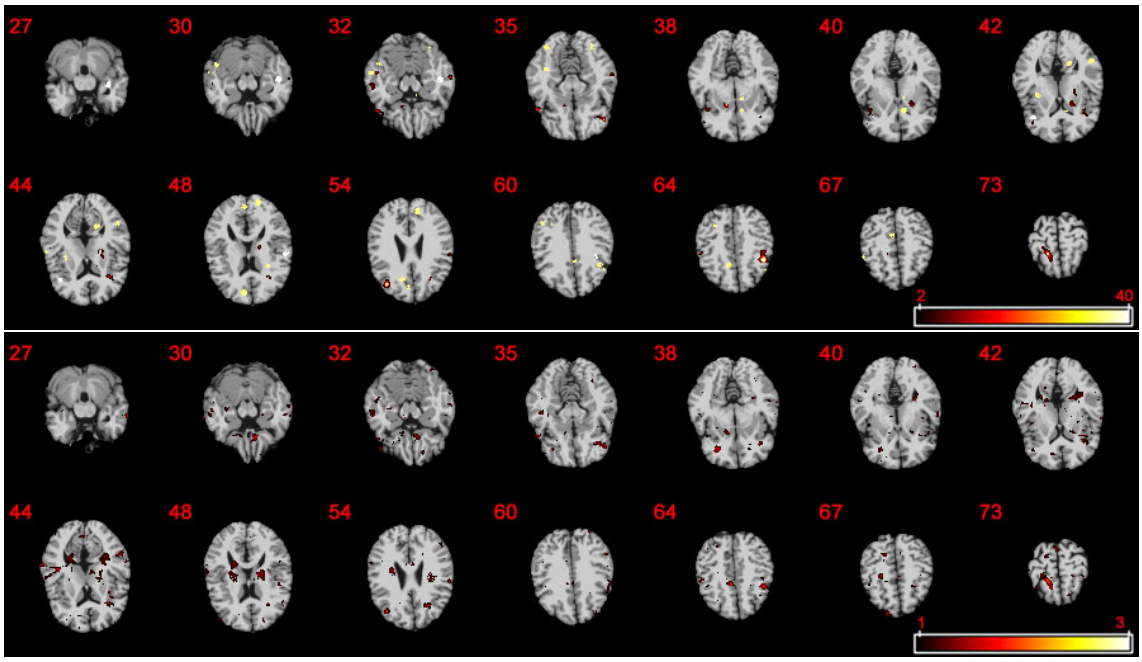

Figure 3: ADNI data analysis based on the combined HC and AD samples: the $-\log_{10}(p)$ maps for testing the genetic effect of **CR1** on RAVEN images by using FMEM from 14 selected slices. The first and second rows are obtained from FMEM, while the third and fourth rows are obtained from Ge's method. The colorbar of $-\log_{10}(p)$ ranges from 2 to 40 for FMEM and from 1 to 3 for Ge's method, respectively.

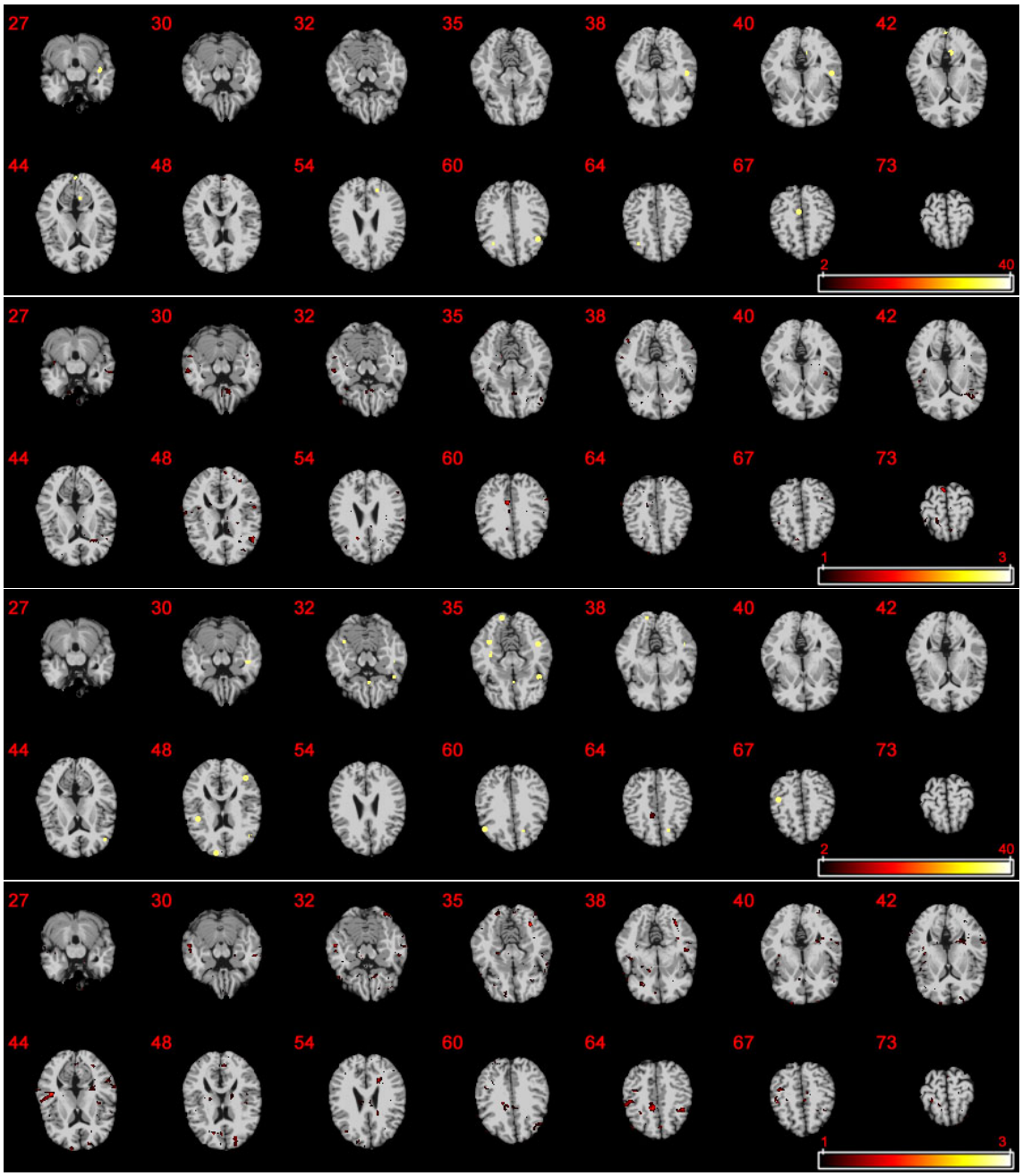

Figure 4: ADNI data analysis based on either AD samples (the first four rows) or HC samples (the last four rows): the $-\log_{10}(p)$ maps for testing the genetic effect of **CR1** on RAVEN images by using FMEM from 14 selected slices. The first, second, fifth, and sixth rows are obtained from FMEM, while the third, fourth, seventh, and eighth rows are obtained from Ge's method. The colorbar of $-\log_{10}(p)$ ranges from 2 to 40 for FMEM and from 1 to 3 for Ge's method, respectively.

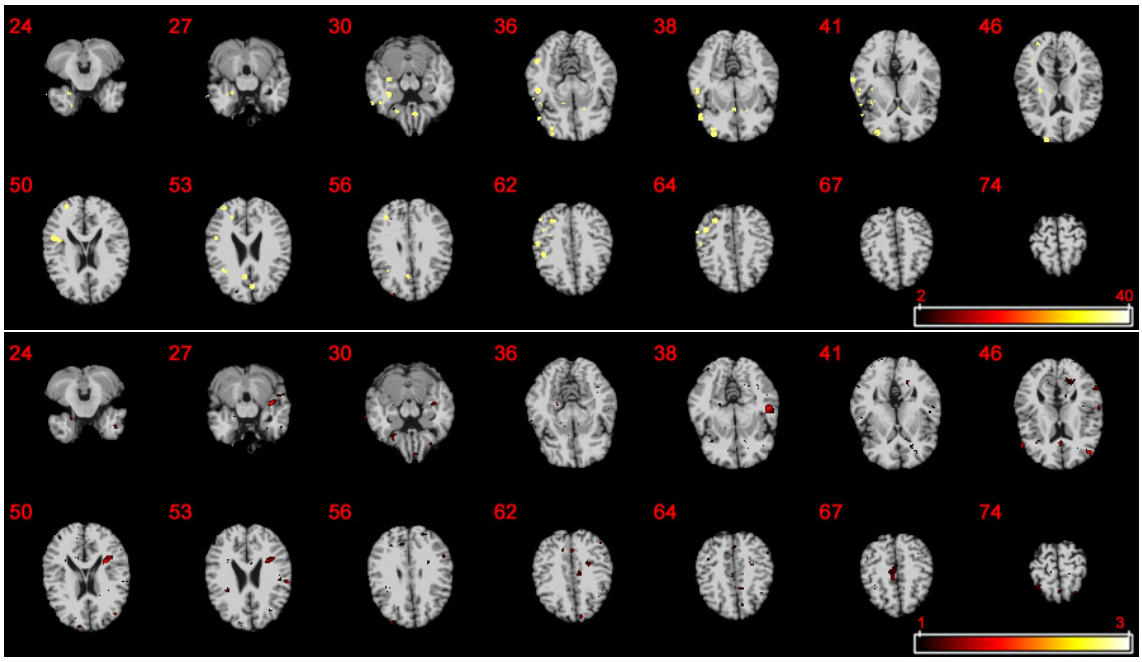

Figure 5: ADNI data analysis based on the combined HC and AD samples: the $-\log_{10}(p)$ maps for testing the genetic effect of **PICALM** on RAVEN images by using FMEM from 14 selected slices. The first and second rows are obtained from FMEM, while the third and fourth rows are obtained from Ge's method. The colorbar of $-\log_{10}(p)$ ranges from 2 to 40 for FMEM and from 1 to 3 for Ge's method, respectively.

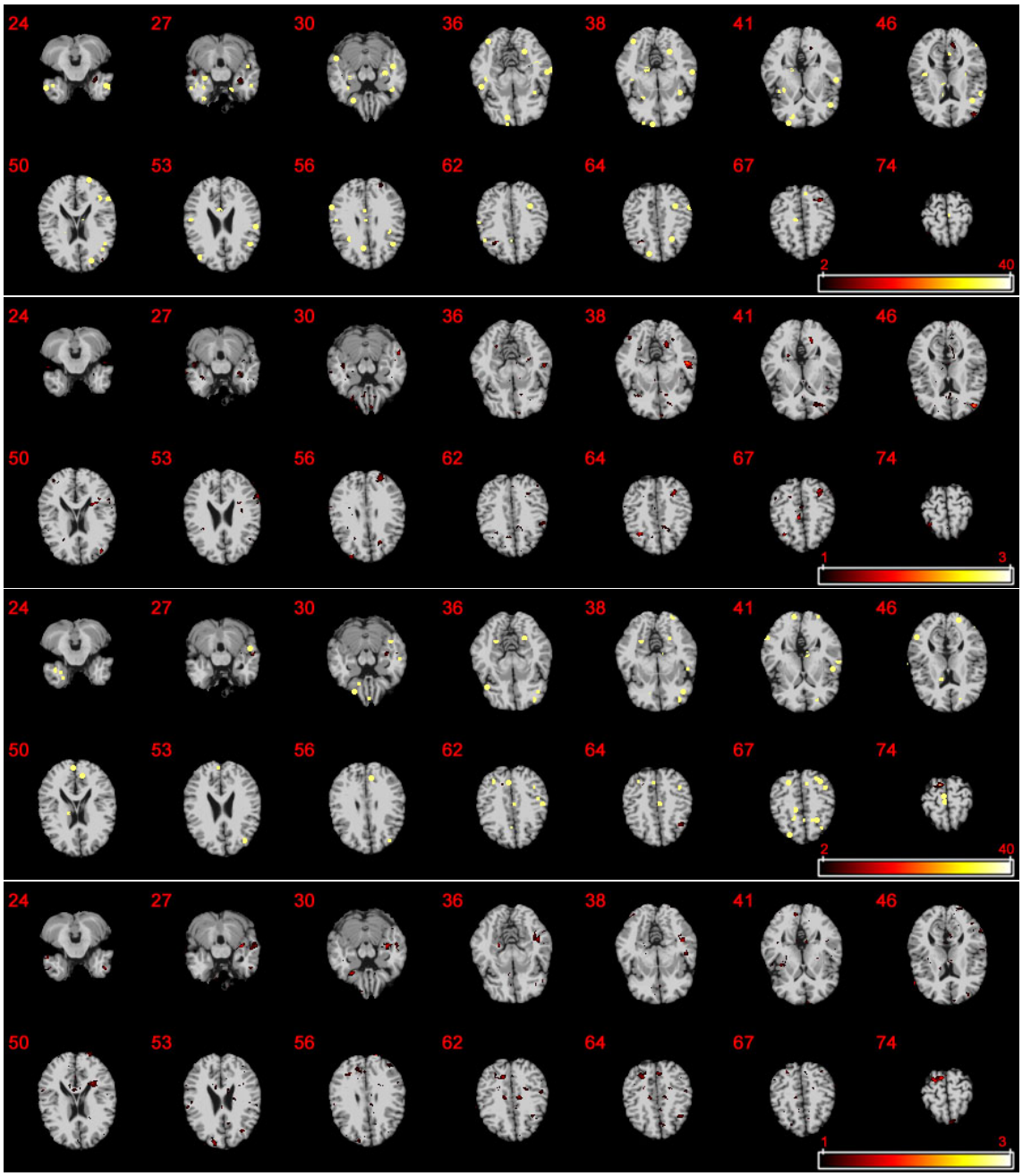

Figure 6: ADNI data analysis based on either AD samples (the first four rows) or HC samples (the last four rows): the $-\log_{10}(p)$ maps for testing the genetic effect of **PICALM** on RAVEN images by using FMEM from 14 selected slices. The first, second, fifth, and sixth rows are obtained from FMEM, while the third, fourth, seventh, and eighth rows are obtained from Ge's method. The colorbar of $-\log_{10}(p)$ ranges from 2 to 40 for FMEM and from 1 to 3 for Ge's method, respectively.